THE JOURNAL OF PHYSICAL CHEMISTRY B LETTERS

2005, *109,* 21481−21485
Published on Web 10/28/2005

Concentration Polarization-based Nonlinear Electrokinetics in Porous Media: Induced-Charge Electroosmosis

Felix C. Leinweber and Ulrich Tallarek*

Institut für Verfahrenstechnik, Otto-von-Guericke-Universität Magdeburg, Universitätsplatz 2, 39106 Magdeburg, Germany

Received: September 27, 2005; In Final Form: October 17, 2005

We have investigated induced-charge electroosmotic flow in a fixed bed of ion-permselective glass beads by quantitative confocal laser scanning microscopy. Externally applied electrical fields induce concentration polarization (CP) in the porous medium due to coupled mass and charge transport normal to the charge-selective interfaces. These data reveal the generation of a nonequilibrium electrical double layer in the depleted CP zones and the adjoining anodic hemispheres of the (cation-selective) glass beads above a critical field strength. This initiates CP-based induced-charge electroosmosis along curved interfaces of the quasi-electroneutral macropore space between glass beads. Caused by mutual interference of resulting nonlinear flow with (flow-inducing) space charge regions, an electrohydrodynamic instability can appear locally and realize turbulent flow behavior at low Reynolds numbers. It is characterized by a local destruction of the CP zones and concomitant removal of diffusion-limited mass transfer. More efficient pore-scale lateral mixing also improves macroscopic transport, which is reflected in the significantly reduced axial dispersion of a passive tracer.

In the classical description, electroosmotic flow (EOF) along a charged solid−liquid interface is generated by interaction of the local tangential components of an applied d.c. electrical field with the net volume charge in the fluid-side electrical double layer (EDL).[1] Volumetric EOF is linear with respect to the applied field strength, laminar, and stationary because the Reynolds number is usually very small.[2] This description has been verified extensively for systems with a locally thin, quasi-equilibrium EDL which remains unaffected by the applied field.[3] It covers EOF through open-channel geometries,[2,4] as well as model porous media consisting of hard (impermeable, nonconducting) spheres.[5] In more complex, hierarchically structured materials represented, e.g., by a fixed bed of permeable, conducting particles, the classical picture can become substantially modified. The coupled mass and charge transport then is influenced by electrical field-induced concentration polarization (CP).[6,7]

This CP phenomenon is related to the formation of concentration gradients of charged species (simple ions, analyte molecules, or globular and colloidal particles) in the electrolyte solution adjacent to an ion-permselective (charge-selective) interface upon the passage of electrical current normal to that interface.[8] In a fixed bed of mesoporous particles it addresses species transfer from the macropore space between particles into the intraparticle mesopore space.[9] While the former is quasi-electroneutral because the macropore sizes are much larger than a typical EDL thickness, the latter becomes charge-selective due to pore-scale EDL interaction as the mesopore sizes are comparable to the EDL thickness. This leads to the favored transfer of counterionic species and exclusion of co-ions.[10] CP induced by a superimposed electrical field due to the local interplay of electromigration, diffusion, and convection then stands for a dynamic deviation of ion concentration distributions in the complete (hierarchically structured) material from those at electrochemical equilibrium.[11−16] Charge transfer through the CP zones becomes diffusion-limited due to steep concentration gradients close to the charge-selective interfaces.[7]

While diffusive flux and therefore the overall mass flux into a mesoporous particle (or into the ion-permselective domain, in general) depend relatively little on the applied field strength via the generated volumetric EOF and local thickness of the diffusion boundary layer, intraparticle charge transport (or transport within the ion-permselective domain, in general) due to mainly electromigration and typically weak electroosmosis shows a much stronger dependence.[8] As a consequence, a critical field strength is approached for which electrokinetic transport within the charge-selective domain begins to exceed diffusive species flux into this domain.[17] Then, local deviation from electroneutrality can occur at that interface where counterions enter the charge-selective domain in the direction of the applied field. It generates an electrokinetically induced secondary, nonequilibrium EDL.[17] The relevant conditions are classified as nonlinear or nonequilibrium and account for a CP-based nonlinear electrokinetics.[17−25] The peculiarity of this electrokinetics is that the classical, primary EDL is complemented by the secondary EDL, which depends on both local dimension and charge density on the applied field strength.[23] As a consequence, the local EOF velocities become nonlinear.[20] Most literature on this nonlinear electrokinetics has been dealing with

* To whom correspondence should be addressed. Fax: +49-(0)391-67-12028; E-mail: ulrich.tallarek@vst.uni-magdeburg.de.

10.1021/jp055491u CCC: $30.25

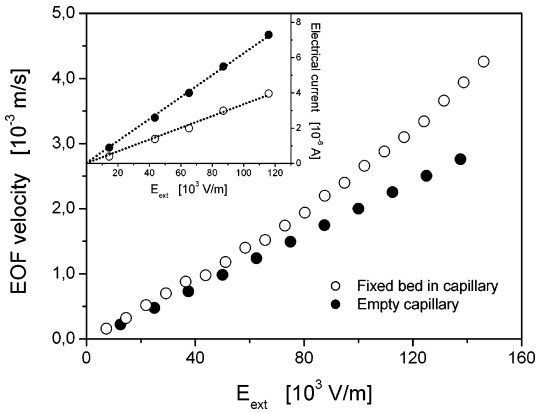

Figure 1. Average interparticle EOF velocities in a fixed bed of ion-permselective, i.e., charge-selective glass beads (particle diameter, $d_p = 100-200\ \mu m$) against the externally applied field strength. Velocities in the empty (unpacked) glass capillary with a quadratic cross-section of $300 \times 300\ \mu m$ are included for comparison. Mobile phase used for solid−liquid refractive index matching in the porous medium consists of 90:10 dimethyl sulfoxide/water with a 10^{-3} M sodium acetate buffer at pH 5.

the electrohydrodynamics evolving in systems of single, spherical-shaped ion-exchange particles (immobilized in closed electrolysis cells),[22,23] as well as with the charge transport through flat ion-exchange membranes for explaining overlimiting conductance behavior in electrodialysis.[24] In this letter, by contrast, we demonstrate effects of nonlinear electrokinetic conditions on the local and bulk transport within a macroscopically charge-nonselective fixed bed of charge-selective glass beads. Visualization and analysis of the electrohydrodynamics revealing the induction and operation of a nonequilibrium EDL was realized by confocal laser scanning microscopy (CLSM) employing refractive index matching. It allows a quantitative analysis of spatio-temporal tracer distributions inside the hierarchically structured material.

Mesoporous glass beads were fixed in a custom-made microfluidic device which enables the application of external electrical fields (E_{ext}) above 10^5 V/m, while the transport of fluorescent tracer molecules is investigated directly using a conventional CLSM system.[26,27] In contrast to the EOF dependence in the empty glass capillary saturated only with electrolyte solution, the interparticle EOF velocities in the same capillary packed with glass beads reveal a nonlinear behavior above $E_{ext} \approx 30$ kV/m (Figure 1). As confirmed by the linear current−voltage plots in the inset, both systems can be assumed as remaining isothermal. Development of Joule heat thus cannot explain the nonlinear flow dynamics in the sphere packing.

To examine whether a secondary, nonequilibrium EDL with the same polarity as the primary, quasi-equilibrium EDL causes this nonlinearity, the local ion concentration distributions were probed with counterionic fluorescent tracer (Figure 2). As indicated earlier, the mobile phase ionic strength (10^{-3} M) with respect to the mean mesopore diameter (20 nm) causes a strong EDL interaction or so-called overlap in the intraparticle pore space. This leads to enrichment of counterionic species by a glass bead at electrochemical equilibrium ($E_{ext} = 0$ kV/m). When an electrical field is applied, the local charge-selectivity induces CP in the quasi-electroneutral solution of the adjoining macroporous compartment. It generates an enriched CP zone at the cathodic hemisphere and a depleted CP zone at the anodic hemisphere of a cation-selective glass bead (Figure 2).[9] This is shown by concentration profiles of counterionic tracer which, inside a bead, are tilted in the field direction ($E_{ext} = 14.4$ kV/m) due to diffusive backflux from the enriched CP zone.

Despite intensifying polarization patterns at increasing field strength, unusual details in the stationary tracer distributions are observed for $E_{ext} = 44.4$ kV/m. Darker regions in the anodic hemisphere of a glass bead at the interface to the macroporous compartment are detectable (gray arrows in Figure 2). Counterion concentration here is reduced below values expected from electrochemical equilibrium, as indicated by the gray-shaded

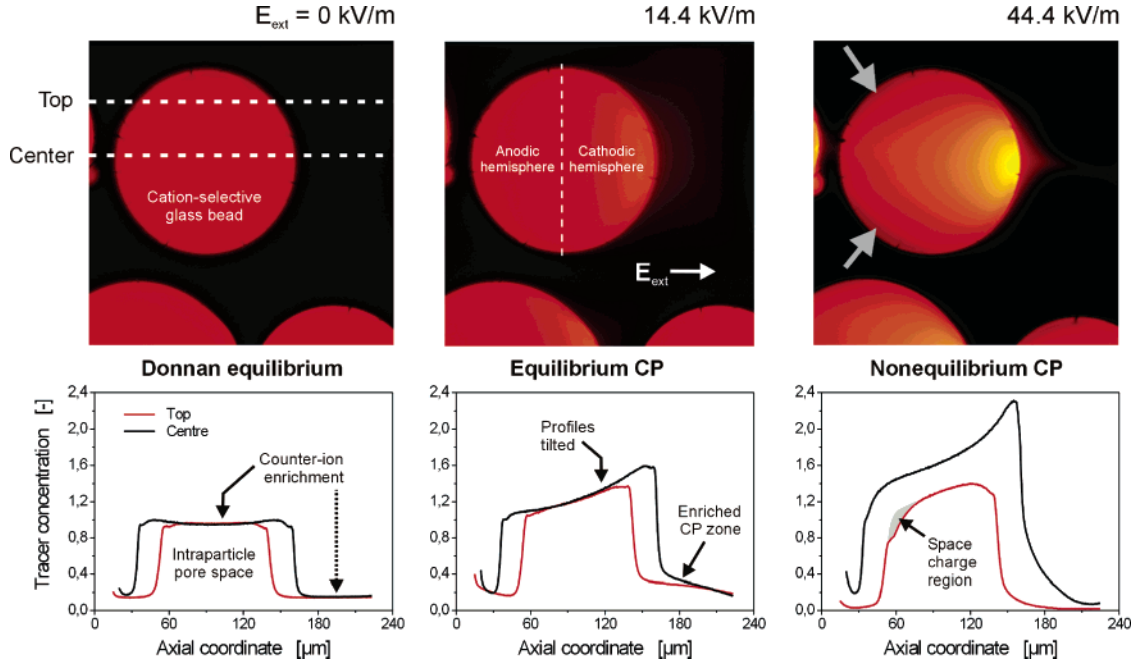

Figure 2. Stationary concentration distributions of a counterionic fluorescent tracer (positively charged Rhodamine 6G, concentration: 10^{-5} M) in and around a glass bead of the fixed bed. The axial profiles represent tracer concentration along indicated top (red lines) and center (black lines) positions in the selected bead and the adjoining interparticle fluid. Mean intraparticle intensity at electrochemical equilibrium ($E_{ext} = 0$ kV/m) serves as the reference for the normalization of profiles obtained with the externally applied electrical fields. The enriched CP zone along the cathodic interface of a glass bead ($E_{ext} = 14.4$ kV/m) becomes better visible in Figure 3 where the focus is on the electrohydrodynamics in the interparticle macropore space.

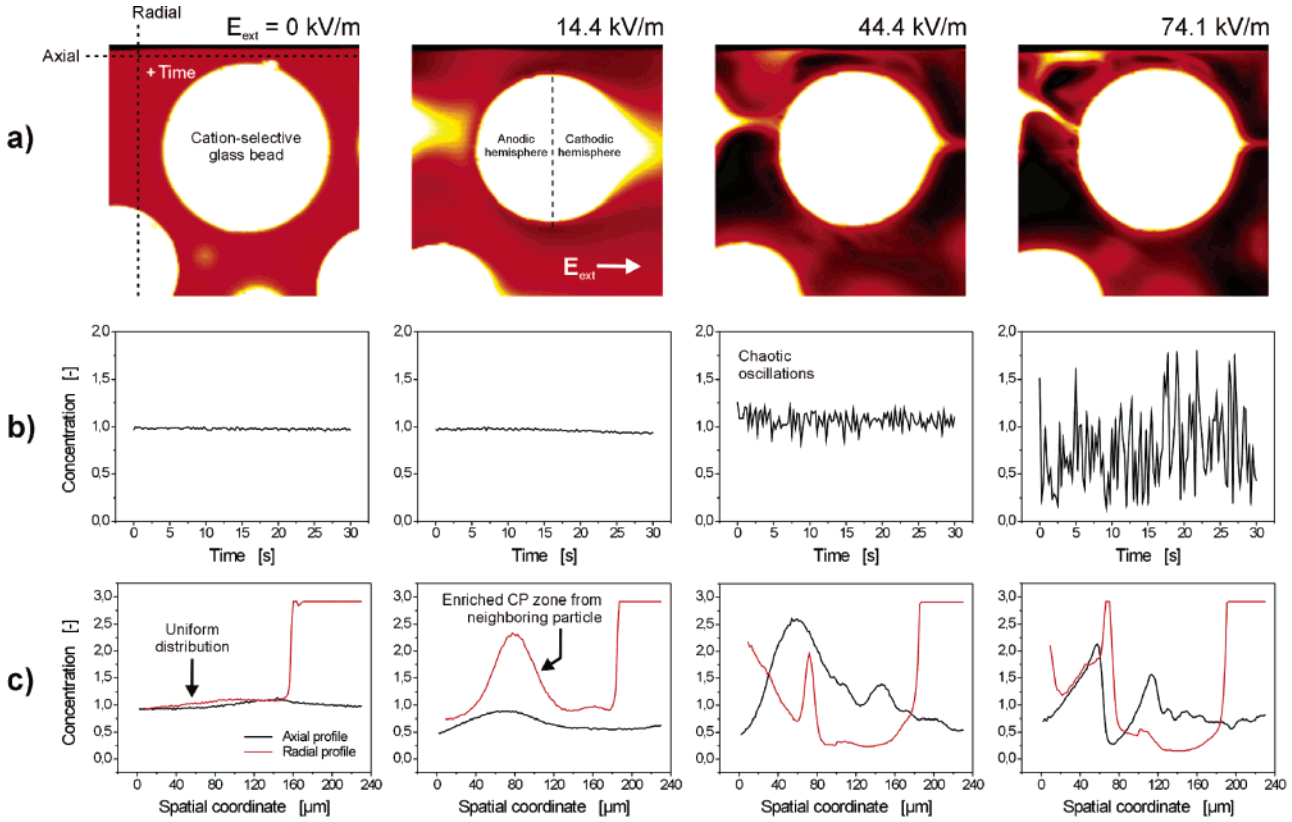

Figure 3. Spatio-temporal distributions of counterionic fluorescent tracer in the interparticle pore space between charge-selective glass beads. (a) Snapshots of the concentration distribution without superimposed electrical field and for selected applied field strengths. (b) Temporal variation of concentration in a particular voxel denoted by the cross. (c) Spatial distribution of tracer along the indicated axial and radial directions. Detector settings were optimized for the interparticle concentration, while intraparticle intensity is beyond the linear range due to tracer adsorption at the oppositely (negatively) charged surface of the glass beads. With a sufficiently high field strength, the enriched CP zones (streamlined, yet stable at $E_{ext} = 14.4$ kV/m) are destroyed by locally chaotic electrohydrodynamic flow. These results also show that in a dense packing of particles, as compared to the single-particle picture in a closed electrolysis cell,[22,23] the actual CP pattern and induced space charge effects become influenced by a significant interference of CP zones from neighboring particles, as well as the hydrodynamics originating in net flow through the system and a higher complexity of the macropore space.

region in the corresponding concentration profile. This decreased concentration seems insufficient for balancing the local inner surface charge of the glass bead, meaning that part of the surface charge then remains unscreened. Thus, these regions ($E_{ext} =$ 44.4 kV/m) point toward an electrokinetically forced deviation from local electroneutrality in the ion-permselective domain.

Regions indicating induced intraparticle space charge can be observed only at field strengths above $E_{ext} \approx 30$ kV/m. For these field strengths, electrokinetic transport inside the glass beads exceeds diffusion-limited transport into a bead through its anodic interface.[17] This means that below a critical field strength local electroneutrality is preserved on the particle-scale, but with higher field strength a space charge region of unscreened surface charge is electrokinetically induced inside a particle. To preserve electroneutrality, the formation of the co-ionic, immobile space charge in the glass bead must be compensated by counterionic space charge outside the charge-selective domain in the electrolyte solution, because double layers as a whole are electroneutral. The counterionic, mobile space charge stimulates nonlinear (induced-charge) electroosmosis and is detected in the macroscopic EOF dynamics (Figure 1). Comparison of these velocity data with the spatially resolved concentration profiles in Figure 2 reveals close correlation between deviation from local electroneutrality and nonlinear electroosmosis in the fixed bed of ion-permselective glass beads.

Apart from a nonlinear EOF dynamics, another difference exists between the classical (linear) and this nonequilibrium electroosmosis. Classical EOF is caused by interaction of the applied electrical field with the quasi-equilibrium EDL. Due to strong normal field components close to the solid−liquid interface, the primary EDL remains relatively unaffected by the applied field and resulting electroconvection concerning both local charge density and spatial dimensions. Steady, laminar EOF develops revealing a linear dependence of the flow rate on applied field strength. For induced-charge electroosmosis the (electrical field-induced) EDL exists more in bulk solution than as a thin and stable layer at the solid−liquid interface. The interaction of the comparatively extended mobile space charge region with the electrical field then will not only cause incuded-charge electroosmosis (which explains the observed nonlinear dynamics) but can also lead to instability of the flow pattern depending on local resistance and, thus, on the packing density. While the local electrohydrodynamics at field strengths up to $E_{ext} \approx 30$ kV/m is characterized by stationary tracer distributions (Figure 3), randomly fluctuating and spatially nonuniform concentration profiles are observed with higher field strength. These distributions reveal the onset of an interparticle macropore-scale flow instability and local turbulence. This confirms the existence of a critical field strength at which the transition from laminar flow with stationary, considerably streamlined CP zones ($E_{ext} = 14.4$ kV/m) to chaotic flow behavior is realized. Because the deviation from local electroneutrality and a nonlinearity of velocity data have been complementarily demonstrated with Figures 1 and 2, nonequilibrium electroosmosis based on a spatially extended, secondary EDL appears to show turbulent flow characteristics under certain conditions.

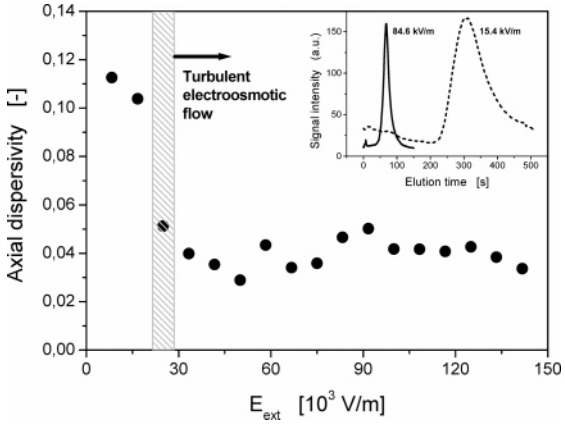

Figure 4. Interparticle fluid-side electrohydrodynamic dispersion in dependence of the applied electrical field strength. Dispersion data are derived from elution signals which follow pulse injection of fluorescent nanoparticles. The dimensionless axial dispersivity relates the second centralized moment to the squared first moment of these signals. As evidenced, for field strengths above $E_{ext} \approx 30$ kV/m, pore-scale dispersion is significantly reduced. The inset shows elution profiles for $E_{ext} = 15.4$ and 84.6 kV/m.

The origin of this general difference between linear and nonlinear electroosmosis is related to the physical nature of flow-inducing space charge regions. As mentioned above, for classical electroosmosis the EDL is firmly attached to the solid−liquid interface by strong normal field components. For nonequilibrium electroosmosis the field-induced EDL is located far more in the bulk solution.[23] This peculiarity has two consequences. First, it means that the secondary EDL is a dynamic, field-dependent property and not just a static material characteristic as the primary EDL. Second, resulting EOF mutually interacts with the mobile space charge regions and thereby affects their spatio-temporal dimension and local charge density. Consequently, the flow regime for nonlinear electrokinetic conditions can become unstable and demonstrate turbulent flow behavior.

To address the impact of this electrokinetic instability resulting in pore-scale turbulence, axial dispersion was investigated with tracer pulse injections of fluorescent nanoparticles. Due to a mean size of 50 nm they are excluded from the intraparticle mesopore space and, therefore, specifically probe the electrohydrodynamics in the interparticle macropore space. As seen in Figure 4, the axial dispersivity can be strongly reduced by a transition from linear to nonlinear electroosmosis (at $E_{ext} \approx 30$ kV/m). This improvement in zone spreading suggests increased radial dispersion due to a chaotic mixing that is demonstrated in Figure 3. Accelerated lateral equilibration, in turn, reduces axial dispersion. Since the critical field strength for the onset of this improvement coincides with the deviation from local electroneutrality (revealed by Figure 2), these data complement the existence of an efficient pore-scale mixing under the nonlinear electrokinetic conditions by chaotic flow. Analysis of the flow regime shows that the Reynolds numbers $\mathrm{Re} = u_{sf} d_p/\nu$ (where u_{sf} is the superficial velocity, d_p the particle diameter, and ν the kinematic viscosity) with $\mathrm{Re} \approx 0.2$ at the highest are more than a decade below values typical for the onset of turbulence in sphere packing.[28,29] Thus, classical hydrodynamic arguments cannot explain the observed flow instability.[8] Instead, the chaotic flow and mixing is attributed to unique physical properties of induced-charge electroosmosis which realizes turbulent flow behavior already at low Re.

To summarize, CP-based nonequilibrium electroosmosis can be considered as substantially differing from the classical picture of linear, quasi-equilibrium electroosmosis. Particularly, the nonlinear macroscopic EOF dynamics (Figure 1), relatively extended induced space charge regions (Figure 2), flow instability (Figure 3), and the resulting pore-scale dispersion (Figure 4) constitute key differences. Thus, induced-charge electroosmosis can become a promising tool for process intensification, e.g., in electrodialysis (membrane transport) which is severely limited by stable CP,[24,30] or in miniaturized devices concerning the nonlinear pumping of bulk fluid[31] and efficient mixing at low Re, i.e., $\mathrm{Re} < 1$.[2,3] In separation science, the realization and control of chaotic instability and turbulent flow over defined temporal and spatial domains has been a challenging task for a long time.[32−34] In this respect, nonlinear electrokinetics analyzed in this letter is a unique mechanism for reducing axial dispersion by faster lateral exchange of analytes beween flow velocity extremes during the long-distance transport through porous media employed, e.g., in electrochromatography. Future work needs to address the influence of the applied field and mobile phase ionic strengths, local hydrodynamics, morphology of the pore space, and surface physicochemical properties on the development and consequences of induced-charge electroosmosis in porous media.

Acknowledgment. This work was supported by the Deutsche Forschungsgemeinschaft (Bonn, Germany) under grants SE 586/7-2 and TA 268/1-1, as well as by Fonds der Chemischen Industrie (Frankfurt a.M., Germany).

References and Notes

(1) Lyklema, J. *Fundamentals of Interface and Colloid Science, Vol. II: Solid−Liquid Interfaces*; Academic Press: San Diego, 1995.

(2) Li, D. *Electrokinetics in Microfluidics*; Academic Press: Oxford, 2004.

(3) Stone, H. A.; Stroock, A. D.; Ajdari, A. *Annu. Rev. Fluid Mech.* **2004**, *36*, 381.

(4) Santiago, J. G. *Anal. Chem.* **2001**, *73*, 2353.

(5) Hlushkou, D.; Seidel-Morgenstern, A.; Tallarek, U. *Langmuir* **2005**, *21*, 6097.

(6) Helfferich, F. *Ion Exchange*; Dover Publications: New York, 1995.

(7) Sørensen, T. S., Ed. *Surface Chemistry and Electrochemistry of Membranes*; Marcel Dekker: New York, 1999.

(8) Probstein, R. F. *Physicochemical Hydrodynamics*; John Wiley & Sons: New York, 1994.

(9) Leinweber, F. C.; Pfafferodt, M.; Seidel-Morgenstern, A.; Tallarek, U. *Anal. Chem.* **2005**, *77*, 5839.

(10) Lyklema, J. *Phys. Rev. E* **2005**, *71*, art. no. 032501.

(11) Mandersloot, W.; Hicks, R. E. *Ind. Eng. Chem. Proc. Des. Dev.* **1965**, *4*, 304.

(12) Seno, M.; Yamagata, K.; Shinoda, J.; Yamabe, T. *J. Electrochem. Soc. Jpn.* **1966**, *34*, 232.

(13) Forgacs, C.; Ishibashi, N.; Leibovitz, J.; Sinkovic, J.; Spiegler, K. S. *Desalination* **1972**, *10*, 181.

(14) Khedr, G.; Varoqui, R. *Ber. Bunsen-Ges. Phys. Chem.* **1981**, *85*, 116.

(15) Tanaka, Y. *J. Membr. Sci.* **1991**, *57*, 217.

(16) Manzanares, J. A.; Kontturi, K.; Mafé, S.; Aguilella, V. M.; Pellicer, J. *Acta Chem. Scand.* **1991**, *45*, 115.

(17) Leinweber, F. C.; Tallarek, U. *Langmuir* **2004**, *20*, 11637.

(18) Dukhin, S. S. *Adv. Colloid Interface Sci.* **1991**, *35*, 173.

(19) Manzanares, J. A.; Murphy, W. D.; Mafé, S.; Reiss, H. *J. Phys. Chem.* **1993**, *97*, 8524.

(20) Mishchuk, N. A.; Takhistov, P. V. *Colloids Surf. A* **1995**, *95*, 119.

(21) Rubinstein, I.; Zaltzmann, B. *Phys. Rev. E* **2000**, *62*, 2238.

(22) Ben, Y.; Chang, H.-C. *J. Fluid Mech.* **2002**, *461*, 229.

(23) Mishchuk, N. A.; Dukhin, S. S. In *Interfacial Electrokinetics and Electrophoresis*; Delgado, A. V., Ed.; Marcel Dekker: New York, 2002; pp 241−275.

(24) Rubinshtein, I.; Zaltzmann, B.; Pretz, J.; Linder, C. *Russ. J. Electrochem.* **2002**, *38*, 853.

(25) Ben, Y.; Demekhin, E. A.; Chang, H.-C. *J. Colloid Interface Sci.* **2004**, *276*, 483.

(26) Tallarek, U.; Rapp, E.; Sann, H.; Reichl, U.; Seidel-Morgenstern, A. *Langmuir* **2003**, *19*, 4527.

(27) Tallarek, U.; Pačes, M.; Rapp, E. *Electrophoresis* **2003**, *24*, 4241.
(28) Takatsu, Y.; Masuoka, T. *J. Porous Media* **1998**, *1*, 243.
(29) Knox, J. H. *J. Chromatogr. A* **1999**, *831*, 3.
(30) Ibanez, R.; Stamatialis, D. F.; Wessling, M. *J. Membr. Sci.* **2004**, *239*, 119.
(31) Yao, S.; Santiago, J. G. *J. Colloid Interface Sci.* **2003**, *268*, 133.
(32) Pretorius, V.; Smuts, T. W. *Anal. Chem.* **1966**, *38*, 274.
(33) Giddings, J. C.; Manwaring, W. A.; Myers, M. N. *Science* **1966**, *154*, 146.
(34) Sumpter, S. R.; Lee, M. L. *J. Microcolumn Sep.* **1991**, *3*, 91.